https://doi.org/10.5194/essd-2026-68
Preprint. Discussion started: 23 March 2026
© Author(s) 2026. CC BY 4.0 License.

Open Access Earth System Science Data Discussions

Revealing coastal vegetation structural diversity through LiDAR-derived relative entropy

Guanpu Qi[1]†, Jiawei Wei[2]†, Zaizhou Xin[3], Longcheng Yao[1], Xiong Chen[2*], Jun Ma[1*]

[1] State Key Laboratory of Wetland Conservation and Restoration, National Observations and Research Station for Wetland Ecosystems of the Yangtze Estuary, Ministry of Education Key Laboratory for Biodiversity Science and Ecological Engineering, and Institute of Eco-Chongming, School of Life Sciences, Fudan University, # 2005 Songhu Road 10, Shanghai, 200438, China.

[2] School of Information Science and Engineering, Fudan University, # 2005 Songhu Road 10, Shanghai, 200438, China.

[3] Key Laboratory of Computational Physical Sciences (Ministry of Education), Institute of Computational Physical Sciences, State Key Laboratory of Surface Physics, and Department of Physics, Fudan University, Shanghai 200433, China.

†These authors contributed to the work equally.

*Corresponding author

E-mail:

Jun Ma: **ma_jun@fudan.edu.cn**

Xiong Chen: **chenxiong@fudan.edu.cn**

Tel. Jun Ma: +86-21-31246690.

Tel. Xiong Chen: +86-21-65643231.

https://doi.org/10.5194/essd-2026-68
Preprint. Discussion started: 23 March 2026
© Author(s) 2026. CC BY 4.0 License.

Open Access Earth System Science Data Discussions

Abstract. Coastal wetlands are among the most valuable ecosystems globally, due to the high ecological function of their structurally complex vegetation communities. However, there remains a lack of vegetation structural complexity (VSC) indicators tailored for coastal wetland applications. Here, we developed a new VSC index, vegetation structure relative entropy (VSRE), based on a measure of the asymmetry of the difference between two probability distributions. While the currently used VSC index all fail to capture the discrete and continuous complexity gradients of coastal vegetation communities, VSRE demonstrated ideal performance in these applications, exhibiting strong robustness across varying point cloud densities. By applying this indicator to 1,337 LiDAR samples of natural coastal vegetation, we used Alpha Earth Foundation data and a deep learning model to create a seamless VSRE spatial map of coastal wetlands in China at high spatial resolution (10 m) and high accuracy (R^2 = 0.96). VSRE mapping provides crucial ecosystem structural information beyond vegetation classification data and conventional optical indices, highlighting the high spatial heterogeneity of VSC in coastal wetlands. This study offers a valuable foundation for prioritizing conservation areas and enhancing the resolution and accuracy of coastal zone ecological modelling.

https://doi.org/10.5194/essd-2026-68
Preprint. Discussion started: 23 March 2026
© Author(s) 2026. CC BY 4.0 License.

Open Access Earth System Science Data Discussions

1 Main

1.1 Introduction

Coastal wetlands, including saltmarshes, mangroves, and tidal flats, are among the world's most valuable ecosystems, rich in ecosystem services(Costanza et al., 1997). They not only fix and stabilize blue carbon at a rate far exceeding that of terrestrial ecosystems(Mcleod et al., 2011), which significantly mitigates climate change(Temmerman et al., 2013), but also defend shorelines from storms, purify water quality, and nurture fishery resources, thus bringing substantial benefits to coastal residents(He et al., 2025). In coastal ecosystems, these useful functions and services are realized by different functional groups of vegetation. The differences in the their abilities to provide ecosystem services are determined by the structures of these groups(Lafond-Hudson and Sulman, 2023), that is, "structure determines function", which has been extensively confirmed by studies at scales from individuals to ecosystems(Holling, 1987; Chambers et al., 2007; Robinson et al., 2010; Loreau et al., 2001). Therefore, effectively and objectively quantifying the structural characteristics of coastal wetlands enables us to better estimate and predict ecosystem service provision.

Light detection and ranging (LiDAR) technology efficiently captures detailed structural information about ground features (Guo et al., 2020) and demonstrates superior capability for characterizing vegetation structure compared to traditional optical and radar methods(Dassot et al., 2011). LiDAR monitoring generates accurate spatial representations of plant structural elements as point clouds through high-precision, three-dimensional positioning measurements(Lohani and Ghosh, 2017). Numerous indicators of vegetation structural complexity (VSC) have been developed over time using LiDAR data to quantify ecosystem structural attributes(Bergen et al., 2009). Examples of indices

https://doi.org/10.5194/essd-2026-68
Preprint. Discussion started: 23 March 2026
© Author(s) 2026. CC BY 4.0 License.

Open Access Earth System Science Data Discussions

recognized as effective in quantifying vegetation structure include the horizontal structural index (canopy coverage)(Tang et al., 2019), the vertical structural index (foliage height diversity)(Macarthur and Macarthur, 1961), and integrated indices such as canopy rugosity(Parker and Russ, 2004), fractal dimension(Theiler, 1990), and canopy entropy(Liu et al., 2024). Among these, integrated VSC indices comprehensively quantify both vertical and horizontal structural attributes, exhibit broad applicability and representativeness, thereby dramatically enhancing our understanding of terrestrial ecosystems represented by forests (Ehbrecht et al., 2021). However, their potential application in coastal wetlands has not yet been explored, which has become a key factor limiting our understanding of their relationship with ecosystem function and structural characteristics.

A significant ecological characteristic of coastal wetlands is their periodic inundation by ocean tides and their soft, muddy, or organic soils, which contain abundant water and salt (He et al., 2025; Yando et al., 2023). This unique environment supports vegetation communities typically characterized by open-canopy succulents, graminoids, and mangroves, which differ substantially from terrestrial forest ecosystems(Lafond-Hudson and Sulman, 2023). Although coastal wetland vegetation generally exhibits lower average height and species diversity per unit area compared to forest ecosystems(Simard et al., 2019; He et al., 2025), the interference introduced by dense mixtures of herbaceous and woody vegetation, as well as interspersed water surfaces(Moffett et al., 2015), simultaneously imposes unprecedented demands on the sensitivity and robustness of VSC indicators. Additionally, challenging field conditions in coastal wetlands limit the collection of empirical survey data (Webb et al., 2013), resulting in very few studies testing the effectiveness of existing VSC indicators in coastal settings (Weilhoefer, 2011) and even fewer developing indicators specifically adapted to coastal ecosystems.

https://doi.org/10.5194/essd-2026-68
Preprint. Discussion started: 23 March 2026
© Author(s) 2026. CC BY 4.0 License.

Open Access Earth System Science Data Discussions

In this study, we used the world's largest water-level-controlled field site on Chongming Island, Shanghai, China (Fig. 1) to develop a LiDAR-based index, termed vegetation structure relative entropy (VSRE), capable of effectively quantifying VSC in coastal wetlands. We segmented the point clouds horizontally using a set of three-dimensional sliding windows with variable scales to capture local and regional features. Voxel-based histograms were statistically modelled within each window to ensure robustness against variations in point cloud density (PCD). VSRE was quantified using relative entropy (RE, also known as the Kullback–Leibler divergence) (Cover and Thomas, 1991), computed vertically within each window, and then averaged across windows to enhance robustness across varying scales. We subsequently applied the VSRE algorithm to 18 field plots (each 60 × 60 m) that were classified into three groups reflecting increasing levels of VSC and tested its discriminative ability at varying point cloud densities.

Furthermore, by integrating vegetation biomass sampling data from these plots, we evaluated whether VSRE exhibited significant correlations with biodiversity across the sampled plots. We conducted similar evaluations for other commonly used VSC metrics to assess VSRE's performance comparatively. Finally, we applied our methodology to LiDAR datasets from 1,336 coastal vegetation sites (covering China's 18,400 km coastline) and corresponding vegetation type data from 2022 to characterize variations in VSC across natural vegetation communities within coastal wetlands. Leveraging the Alpha Earth Foundation (AEF) dataset and deep learning models, we present a high-resolution (10 m) seamless mapping of coastal VSRE.

1.2 Description

1.2.1 LiDAR data collection in the fixed plot and field plots

https://doi.org/10.5194/essd-2026-68
Preprint. Discussion started: 23 March 2026
© Author(s) 2026. CC BY 4.0 License.

Open Access Earth System Science Data Discussions

This study was based on the world's largest water-level-controlled wetland experimental plot, the Dongtan Ecosystem Experimental Plot (**Fig. 1**). Established in 2018, the plot has allowed vegetation to grow entirely under natural coastal wetland conditions. The experimental setup includes three distinct water levels (-30 cm, 0 cm, and +30 cm), randomly distributed across a 130-hectare coastal wetland. The site was divided into 18 secondary plots, each measuring 60 × 60 meters, with two open-top chambers installed within each plot.

Under these conditions, the vegetation communities developed distinct structural types: at the +30 cm tidal level, the community is dominated almost exclusively by *P. australis*; at the 0 cm level, diverse herbaceous species form mixed communities; and at the -30 cm level, mixed herbaceous species coexist with woody plants resembling mangrove structures. These naturally formed communities with contrasting vegetation structures provided ideal experimental conditions for our study.

We conducted LiDAR surveys over the fixed plot using a DJI Matrices 300 RTK drone equipped with an L1 LiDAR sensor. Each flight mission covered the entire experimental site to ensure accurate spatial matching. Point cloud densities were controlled by adjusting flight height and overlap rate, targeting approximate densities of 50, 100, 250, 500, 1000, 1500, and 2000 points/m². Datasets collected at 50 and 100 points/m² were discarded due to excessive absorption by water surfaces. Raw LiDAR data were processed in DJI Terra for stitching and denoising, and individual secondary plots (50 × 60 m) were cropped to match the spatial extent of the ground survey plots. During cropping, we prioritized minimizing chamber inclusion while preserving all relevant vegetation features (specific cropping boundaries are shown in **Fig. 1b**).

https://doi.org/10.5194/essd-2026-68
Preprint. Discussion started: 23 March 2026
© Author(s) 2026. CC BY 4.0 License.

In addition, we conducted extensive field surveys along China's coastal zones from 2022 to 2023. We performed numerous scanning missions at major coastal vegetation hotspots using the same drone and LiDAR setup. LiDAR data collection was scheduled during periods of good visibility and low tide to ensure high-quality optical imagery for accurate data cropping. We also supplemented forest LiDAR sampling in Yunhe City, Zhejiang Province, using the same equipment and parameters to improve the dataset contrast. Across all sites, the collected point cloud densities ranged from 20.89 to 4364.33 points/m², with an average density of 790.22 points m^{-2}.

https://doi.org/10.5194/essd-2026-68
Preprint. Discussion started: 23 March 2026
© Author(s) 2026. CC BY 4.0 License.

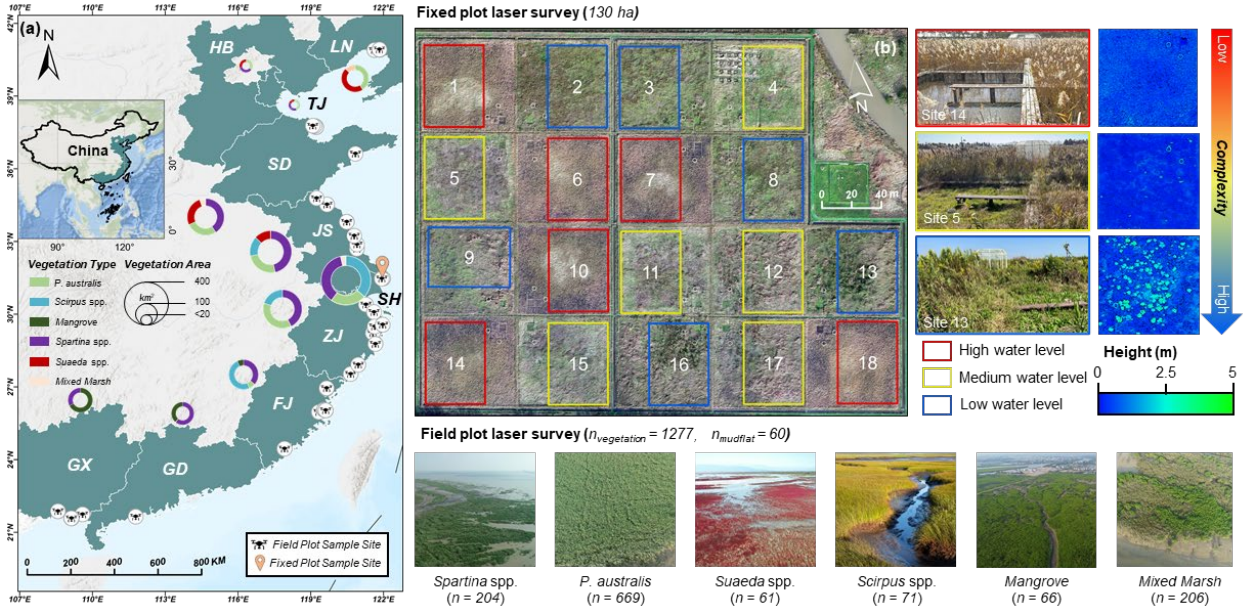

Fig. 1 | Overview of fixed plots and spatial layout of field drone sampling sites. a, Spatial distribution of all LiDAR sampling locations. Blue-green shading indicates sampled provinces, abbreviated with two-letter codes; drone icons represent the field LiDAR sampling sites, and the orange icon indicates the location of the fixed sampling site. **b**, LiDAR sampling conditions within fixed plots and primary vegetation communities surveyed. The LiDAR acquisition ranges under varying water levels are illustrated using three-color boxes, indicating that VSC decreases significantly as tidal levels rise. Representative field photos and digital surface elevation profiles from three sampling points are displayed on the right. Field-collected LiDAR data encompass six typical coastal wetland vegetation types, including succulent herbs (*Suaeda* spp., *Scirpus* spp.), graminoid vegetation (*Phragmites australis*, *Spartina* spp.), mixed marsh communities, and tree-dominated communities (mangroves).

1.2.2 Fieldwork and quantitative VSC calculation

Because environmental conditions across secondary plots were spatially similar, herbaceous vegetation exhibited relatively homogeneous growth patterns. Therefore, a tertiary sampling plot measuring 5 × 5 meters was established in the corner of each secondary plot to represent herbaceous vegetation for biomass assessment. In September 2024, we randomly deployed three 0.5 × 0.5 m quadrats within each tertiary plot to sample herbaceous plants for species identification. The sampled herbaceous vegetation

https://doi.org/10.5194/essd-2026-68
Preprint. Discussion started: 23 March 2026
© Author(s) 2026. CC BY 4.0 License.

Open Access Earth System Science Data Discussions

was oven-dried at 70°C until a constant weight was achieved; this final weight was recorded as the biomass per unit area for herbaceous plants.

For trees, we used the canopy height model (CHM) in LiDAR 360 software to segment individual trees across the fixed plots and assigned each segmented tree to its corresponding secondary plot(Fischer et al., 2019). Each tree extracted by the segmentation algorithm was associated with diameter measurements at breast height (DBH) and crown height. Tree species were identified in the field (*Sapium sebiferum* dominated), enabling the selection of appropriate allometric models to estimate biomass. We subsequently calculated the total tree biomass for each secondary plot using species-specific binary allometric models based on DBH and tree height(Jucker et al., 2022).

Due to the dense herbaceous vegetation, even if individual counts were possible, the large discrepancy between herbaceous and tree individuals would make it difficult to apply traditional biodiversity indices accurately. Therefore, we used biomass rather than individual counts to calculate the classic Shannon Diversity Index (Cousins, 1991). Specifically, we summed the biomass of herbaceous and tree species to obtain the total biomass ($Biomass_{total}$) for each secondary plot. The biomass of each species ($Biomass_i$) was then divided by $Biomass_{total}$ to calculate the relative biomass proportion (p_i). Finally, the Shannon Diversity Index (H) was calculated for each secondary plot using Formula 1.

$$H = -\sum P_i \times \ln(P_i) \quad (1)$$

$$P_i = \frac{Biomass_i}{Biomass_{total}} \quad (2)$$

1.2.3 Development of vegetation structure relative entropy

https://doi.org/10.5194/essd-2026-68
Preprint. Discussion started: 23 March 2026
© Author(s) 2026. CC BY 4.0 License.

We employ a 3D sliding-window approach on the terrain-normalized point cloud (Terrain simulation, in **Supplementary Text**) to construct local voxel histograms and use the RE to measure spatial distribution differences between windows, thereby extracting structural complexity at multiple scales. RE is a statistical metric that quantifies the discrepancy between two probability distributions. It characterizes the additional information required to transform a reference distribution into a target distribution, thus providing a robust measure of distributional deviation.

We first normalize the density distributions within sliding windows to mitigate potential biases, thereby reducing the influence of local anomalies (e.g., occlusions, water bodies, or data gaps) and global variations in point density. The VSRE is then computed on these normalized distributions to quantify spatial heterogeneity in a standardized manner. By adjusting scale-specific sliding intervals and window sizes, our algorithm enhances the continuity of local features, enabling a spatially explicit assessment of VSC.

Let $\tilde{\mathcal{P}} = \{(x_i, y_i, z_i - \hat{z_i})\}_{i=1}^{N}$ represent the terrain-eliminated point cloud data. Where $\hat{z} = f(x, y)$ is the estimated terrain height. To capture local variations in point density and spatial structure, the terrain-normalized point cloud is divided into 3D windows. Let $\mathcal{W}(\mathrm{x}, \mathrm{y}, \mathrm{z})$ be a window in space with ranges $(\mathrm{L_x}, \mathrm{L_y}, \mathrm{L_z})$. The segmentation of $\tilde{\mathcal{P}}$ is performed using a sliding window approach, where the window boundaries are defined as:

$$\begin{cases} x \in [m_x \cdot (1-o) \cdot L_x, (m_x+1) \cdot (1-o) \cdot L_x] \\ y \in [m_y \cdot (1-o) \cdot L_y, (m_y+1) \cdot (1-o) \cdot L_y] \\ z \in [m_z \cdot L_z, (m_z+1) \cdot L_z] \end{cases} \quad (3)$$

Where $m_x, m_y, m_z = [1, \ldots, m_{x,y,z}^{max}] \in Z^+$ represent the sliding indices. To further mitigate the impact of water bodies and cracks on the horizontal plane, an overlap factor $o \in [0,1]$ is introduced. This factor

https://doi.org/10.5194/essd-2026-68
Preprint. Discussion started: 23 March 2026
© Author(s) 2026. CC BY 4.0 License.

Open Access Earth System Science Data Discussions

facilitates information sharing between adjacent windows, enhancing the continuity of local features and reducing the boundary effect between windows. By setting windows at different scales, local structural features can be extracted at various spatial resolutions, thus improving the representation of vegetation structure.

To ensure robustness against point cloud variations, the distribution of points within each window is modelled through a 3D histogram. Furthermore, the window is uniformly divided into voxels b with side lengths Δx, Δy, Δz. For the point cloud data $\mathcal{P}_w$ within the window, the 3D histogram is defined as:

$$H(i,j,k) = \frac{|\{(x_n, y_n, z_n) | (x_n, y_n, z_n) \in b_{ijk}\}|}{|\mathcal{P}_w|} \tag{4}$$

The histogram is then normalized (Π) to obtain the spatial distribution of points within the current window for subsequent quantification of vegetation structure. We use the RE to measure distributional differences across windows. For two distributions, Φ and Ψ representing different sub-windows, the RE for discrete distributions is defined as:

$$RE(\Phi||\Psi) = \sum_{i,j,k} \Phi_{ijk} \log \frac{\Phi_{ijk} + \epsilon}{\Psi_{ijk} + \epsilon} \tag{5}$$

To ensure numerical stability in RE computation and avoid divergence caused by empty voxels or extremely sparse regions (where $\log(0) \to \infty$), we introduce a minimal positive constant ϵ to all probability distributions, thereby eliminating zero-probability elements. In our implementation for field data, we set $\epsilon = 1\mathrm{e} - 43.43$ to standardize the structural complexity metric, constraining all RE scores to a comparable range of 0-100. Although RE is inherently asymmetric and nonlinear, the VSER maintains interpretability by averaging window-level scores. Given that RE's sensitivity to distributional

https://doi.org/10.5194/essd-2026-68
Preprint. Discussion started: 23 March 2026
© Author(s) 2026. CC BY 4.0 License.

differences follows an exponential differential form ($\log(p/q)$), complexity growth exhibits sub-exponential scaling, meaning a doubling of VSER scores reflects a substantial increase in structural heterogeneity (**Supplementary Figure S4**).

For each vertical layer, the RE is computed for all window pairs, yielding the structural diversity score for the current horizontal block. The overall structural complexity score is obtained by averaging the structural diversity scores across all horizontal regions:

$$VSRE = \frac{1}{m_x^{max} \cdot m_y^{max}} \sum^{m_x^{max}} \sum^{m_y^{max}} \frac{1}{m_z^{max} \cdot (m_z^{max} - 1)} \sum_{\substack{i,j=1 \\ i \neq j}}^{m_z^{max}} KL(\Pi_i || \Pi_j) \quad (6)$$

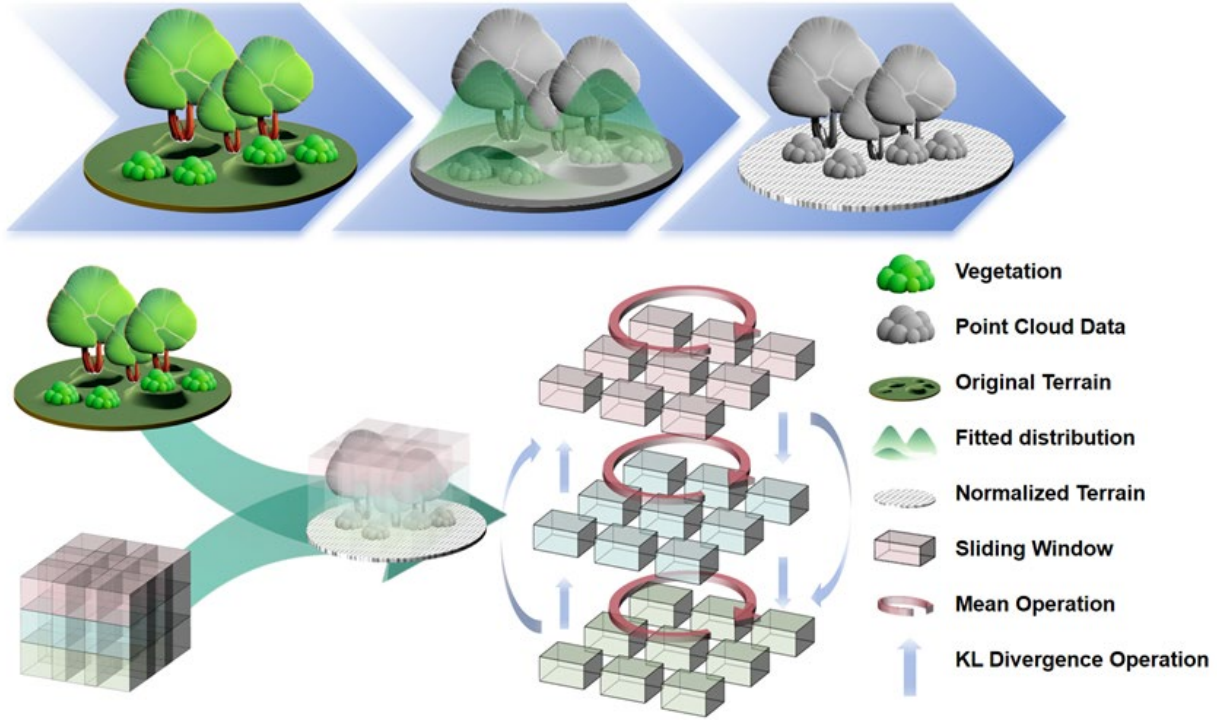

Fig. 2 | Framework of the vegetation 3D structural quantification method based on a sliding window and RE. The figure illustrates key technical processes from raw point clouds to vegetation structural parameter extraction: raw point cloud data undergoes terrain surface fitting and normalization to eliminate topographic relief; 3D sliding windows segment the

https://doi.org/10.5194/essd-2026-68
Preprint. Discussion started: 23 March 2026
© Author(s) 2026. CC BY 4.0 License.

space to construct local voxel probability distributions; RE quantifies spatial heterogeneity by computing RE between adjacent window distributions, characterizing VSC.

1.2.4 Comparison analysis with existing VSC metrics

To further evaluate the effectiveness of VSRE in characterizing vegetation structural complexity (VSC) in coastal saltmarshes, we compared VSRE with several commonly used LiDAR-derived structural metrics that represent different aspects of vegetation structure. These metrics were selected to cover horizontal, vertical, and integrated three-dimensional structures, thereby providing a comprehensive benchmark for assessing the added value of VSRE. All structural metrics were derived from terrain-normalized LiDAR point clouds using a consistent processing workflow to ensure comparability across indices. For each LiDAR sample, ground points were first identified and used to construct a digital terrain model with a 1 m spatial resolution. The original point clouds were then normalized by subtracting the terrain surface, and only those returned with non-negative heights were retained for subsequent calculations.

Mean vegetation height was calculated as the average height of all normalized LiDAR returns within each sample, reflecting the overall vertical development of vegetation. Canopy cover was calculated as the proportion of LiDAR returns exceeding a height threshold of 0.2 m, representing the horizontal occupancy of vegetation elements above the ground surface(Atkins et al., 2018). To describe vertical structural heterogeneity, foliage height diversity (FHD) was calculated from the vertical distribution of normalized LiDAR returns(Macarthur and Macarthur, 1961). Point heights were grouped into vertical layers with a thickness of 0.5 m, and the diversity of point occupancy among these layers was used to represent the complexity of vertical vegetation organization. To ensure robustness, samples with insufficient point density were excluded, and empty height layers were not considered in the

https://doi.org/10.5194/essd-2026-68
Preprint. Discussion started: 23 March 2026
© Author(s) 2026. CC BY 4.0 License.


calculation. Integrated canopy surface complexity was further characterized using canopy surface-based metrics. A canopy height model (CHM) was generated at a 0.5 m spatial resolution using a point-to-raster approach. Canopy rugosity was calculated to quantify canopy surface roughness, reflecting the degree of spatial variation in canopy height(Parker and Russ, 2004).

All five structural metrics were calculated for the same LiDAR samples and spatial extents as VSRE. By comparing VSRE with metrics emphasizing horizontal structure (canopy cover), vertical structure (mean vegetation height and FHD), and integrated canopy structure (rugosity and canopy entropy), this analysis provides a systematic evaluation of whether VSRE captures structural information beyond that represented by conventional vegetation structural complexity indices, particularly in the context of coastal saltmarsh ecosystems.

1.2.5 Vegetation classification in coastal China

First, we integrated all Landsat Collection 2 Level-2 TOA data and Sentinel-2 Level-2A-MSI (TOA) data stored in the Google Earth Engine (GEE) platform(Gorelick et al., 2017). The Landsat series data includes all available Landsat 8 Operational Land Imager (OLI) images from the United States Geological Survey, with a spatial resolution of 30m and a ground revisit time of 8 days(Irons et al., 2012). Sentinel-2 data includes all available Sentinel-2A and Sentinel-2B multi-spectral instrument (MSI) images from the European Space Agency, with a spatial resolution of 10m and a ground revisit time of 5 days(Drusch et al., 2012). The dataset has been atmospherically and terrain-corrected, so we used the QA-Pixel cloud quality function and the Cloudless Probability dataset to remove cloud- and shadow-covered pixels from Landsat-8 and Sentinel-2 images, respectively(Frantz et al., 2018). To

https://doi.org/10.5194/essd-2026-68
Preprint. Discussion started: 23 March 2026
© Author(s) 2026. CC BY 4.0 License.


eliminate differences in sensor bands across satellites, we corrected sensor data using the least-squares method, yielding high-quality remote sensing imagery.

Based on literature research and local pre-classification results, we selected the following four vegetation indices as key parameters for classification. They include the Normalized Difference Vegetation Index (NDVI, equation 7), calculated by the difference in absorption between the near-infrared and red bands. NDVI reflects the health and growth of vegetation. Enhanced Vegetation Index (EVI, equation 8): An improved NDVI index that corrects atmospheric and soil noise, efficiently reflecting dense vegetation growth. Normalized Difference Water Index (NDWI, equation 9): Based on the absorption difference in green and near-infrared bands, NDWI indicates surface soil moisture and vegetation cover. Modified Red Edge Chlorophyll Vegetation Index (M-RECl, equation 10): Reflects chlorophyll content in nitrogen-nourished leaves, indicating canopy photosynthetic activity. The results were resampled using triple convolution to standardize image resolution.

$$NDVI = \frac{NIR - RED}{NIR + RED} \tag{7}$$

$$EVI = 2.5 \times \frac{NIR - RED}{NIR + 6 \times RED - 7.5 \times BLUE + 1} \tag{8}$$

$$NDWI = \frac{GREEN - NIR}{GREEN + NIR} \tag{9}$$

$$MRECI = \left(\frac{\left(\frac{NIR}{RED}\right) - 1}{0.7} \right)^2 \tag{10}$$

NIR (845-885nm); RED (630-688nm); BLUE (450-515nm); GREEN (530-590nm)

https://doi.org/10.5194/essd-2026-68
Preprint. Discussion started: 23 March 2026
© Author(s) 2026. CC BY 4.0 License.


The results are resampled into various vegetation indices through cubic convolution to unify the resolution.

Due to the latitudinal diversity of China's coastal zone, relying on the large number of ground samples obtained from our fieldwork, we use 3°-5° (An elastic interval to ensure the integrity of the vegetation hotspot area) as a classification spatial window for targeted parameterization of the machine learning model. In each spatial window, we divided a year into 24 periods of about 15 days and averaged all pixels 15 days before and after each pixel period into the same day to compensate for the pixel loss due to cloud removal. Then, we used the Savitzky-Golay filtering algorithm to smooth the index time series (Chen et al., 2004). It resulted in an annual vegetation index characteristic distribution map with a temporal resolution of 15 days and a spatial resolution of 30m.

Combining field survey data, we extracted annual spectral time series for different vegetation types within each spatial window and identified multiple key classification temporal windows. These temporal windows are easy to identify because our abundant field samples and effective remote sensing data preprocessing allow the highly distinct physiological characteristics of other vegetation types during a specific phenological period to appear sharply in the time series. During these temporal windows (usually three), we calculated the mean of the four indicators for each window and obtained indicators such as the end vegetation growing season (October-December): EVI10-12mean, NDVI10-12mean, mRECI10-12mean, and NDWI11-12mean, which we used as the final classification features. In addition, we added the annual mean and variance for each indicator as classification features, as they help distinguish vegetated areas from mudflats.

https://doi.org/10.5194/essd-2026-68
Preprint. Discussion started: 23 March 2026
© Author(s) 2026. CC BY 4.0 License.


The corresponding vegetation ground samples (vegetation coordinates) are recorded synchronously. The ground samples were randomly divided into 7:2:1 as training, validation, and test sets. We used 10-fold cross-validation to determine the best model parameter settings and excluded classification features with importance values below a specified threshold within a specific spatial window. We finally used the random forest model due to its high efficiency and accuracy(Breiman, 2001). In the test set, all classification accuracy indicators performed well, indicating the robustness of our mapping. The average OA and Kappa of the classification results were 0.942 and 0.959, respectively (**Supplementary Table S3**).

1.2.6 Mapping the VSRE in coastal China

To transition VSRE mapping from a sample-based scale to a wall-to-wall scale, we utilized the recently released Alpha Earth Foundation (AEF) dataset. This dataset provides 64-dimensional, seamless, dimensionless, and normalized spatial data, covering a 50 km buffer zone along the coastline at an annual 10 m resolution. It integrates a variety of data sources, including optical, SAR, LiDAR, meteorological, topographic, and land use information, and employs deep learning-trained, unlabeled embeddings. We extracted AEF data across all bands from 1,337 coastal vegetation laser samples. Several mainstream machine learning and deep learning models were applied, with 10-fold cross-validation used to assess their robustness and generalizability. The GridSearch algorithm was employed to optimize hyperparameters, ultimately facilitating the seamless VSRE spatial mapping of the entire Chinese coastal region in 2022. Ultimately, we selected the MLP model(Pinkus, 1999), which achieved the following accuracy metrics: $R^2 = 0.9613$, RMSE = 2.812, and MAE = 1.946 (**Supplementary Table S5, Supplementary Figure S6**).

https://doi.org/10.5194/essd-2026-68
Preprint. Discussion started: 23 March 2026
© Author(s) 2026. CC BY 4.0 License.


1.2.7 Statistical analysis and software used

To evaluate differences in VSRE, and other vegetation structural metrics among plots with varying VSC, we applied non-parametric statistical approaches throughout the analysis. For each structural metric, differences among vegetation types within each PCD level were assessed using the Kruskal–Wallis test. When significant differences were detected, pairwise comparisons were conducted using Dunn's post hoc tests with multiple-comparison adjustment. To examine overall differences among vegetation types irrespective of PCD, structural metrics were further summarized using group means and standard deviations, and differences were again assessed using the Kruskal–Wallis test followed by Dunn's post hoc comparisons. The relationships between biodiversity and multiple vegetation structural metrics were analyzed using linear regression models separately for each PCD. Biodiversity was treated as the explanatory variable, while each structural metric served as the response variable.

All statistical analyses were performed using R (Version 4.3.2). Figures were generated using Origin Pro 2023 (Version 9.0.0.87), ArcMap Desktop 10.8 (Esri), Adobe Photoshop (Version 25.0, 2023), and Adobe Illustrator (Version 27.9, 2023).

https://doi.org/10.5194/essd-2026-68
Preprint. Discussion started: 23 March 2026
© Author(s) 2026. CC BY 4.0 License.


1.3 Result

1.3.1 Effectiveness of VSRE in quantifying hierarchical coastal VSC

The core concept of VSRE is based on relative entropy (RE), a symmetric measure of the difference between two probability distributions (Cover and Thomas, 1991). Briefly, VSRE quantifies VSC by comparing the spatial distributions of point clouds. Several hyperparameters critically determine the sensitivity of VSRE. Among these, the most significant are the box height and step size in the vertical (Z) direction, which should align with the vegetation height range and minimum growth height within the targeted ecosystem to achieve effective discrimination. Based on our field measurements, the tallest plants in our plots were trees at approximately 5 m, and the shortest were herbs at around 0.5 m; thus, we selected these as the maximum box height and Z-direction step size, respectively. Other hyperparameters were optimized using a grid search (**Supplementary Figures S1 and S2**).

Statistical analyses indicated that vegetation structural complexity (VSC) indicators widely validated in forest ecosystems failed to reliably and accurately differentiate coastal wetland groups with contrasting VSC levels. Vertical complexity metrics, including mean canopy height (**Fig. 3a**, $P < 0.001$) and FHD (**Fig. 3c**, $P < 0.001$), consistently misclassified the medium-VSC group as having the lowest structural complexity and failed to distinguish between the low- and high-VSC groups across varying PCD. The horizontal complexity indicator, canopy cover, achieved statistically significant separation among the three groups; however, it failed to reflect the expected complexity gradient (**Fig. 3b**), limiting its interpretability in coastal wetlands.

Integrated structural metrics did not resolve this limitation. Canopy surface rugosity did not differentiate between low- and medium-VSC groups (**Fig. 3d**), while canopy entropy, often regarded as

https://doi.org/10.5194/essd-2026-68
Preprint. Discussion started: 23 March 2026
© Author(s) 2026. CC BY 4.0 License.

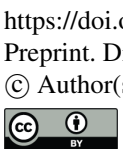

Open Access Earth System Science Data Discussions

a more advanced complexity indicator (**Fig. 3e**), consistently underestimated the complexity of the medium-VSC group. Moreover, the robustness of canopy entropy declined with increasing PCD. When PCD exceeded 1500 points m^{-2}, this metric no longer reliably distinguished between low- and high-VSC groups, indicating reduced sensitivity under high-density sampling conditions. In contrast, VSRE consistently achieved accurate, stable differentiation across groups with distinct VSC gradients. It not only effectively separated groups across increasing levels of complexity but also maintained a robust and coherent relationship across varying point cloud densities (**Fig. 3f**, $P < 0.001$).

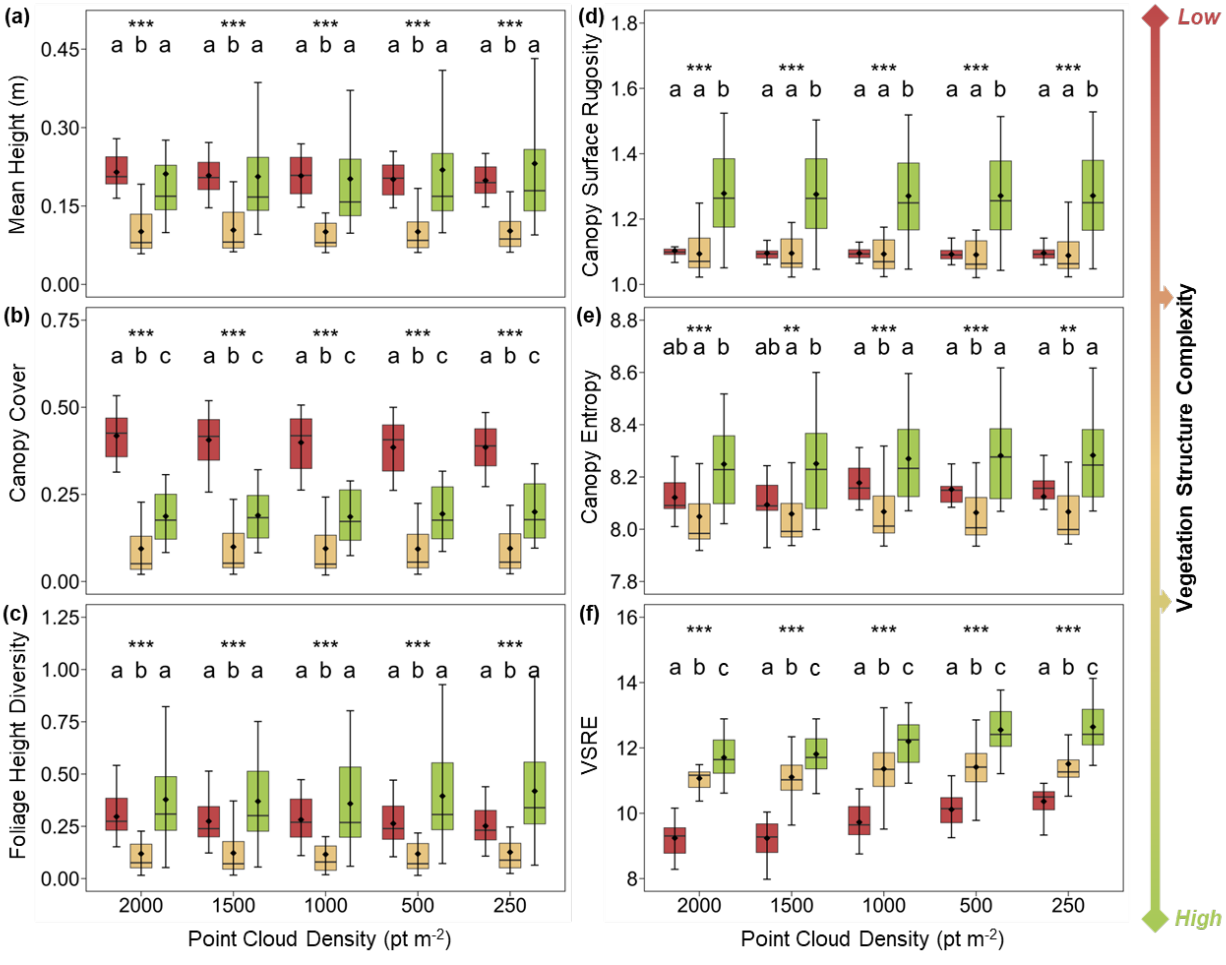

https://doi.org/10.5194/essd-2026-68
Preprint. Discussion started: 23 March 2026
© Author(s) 2026. CC BY 4.0 License.

Fig. 3 | Comparison of the effectiveness of VSRE and other common VSC indicators in distinguishing coastal plots with varying VSC. (a), mean vegetation height; **(b),** canopy cover; **(c)**, FHD (foliage height diversity); **(d)**, canopy rugosity; **(e)**, canopy surface entropy, and **(f)** VSRE. For each metric, statistical differences among the three VSC groups (low, medium, and high) were tested separately within each of the five PCD levels. Within each PCD level, we first applied a Kruskal–Wallis test to evaluate overall group differences, followed by Dunn's post hoc tests with Benjamin–Hochberg correction for pairwise comparisons among different VSC groups. Boxplots show the distribution of metric values for each group within each PCD. The horizontal line inside each box indicates the median, the box bounds represent the interquartile range, and whiskers indicate the non-outlier range (outliers were not displayed). Black diamond markers indicate group means. Different letters above boxes denote significant pairwise differences among groups within the same PCD, while identical letters indicate non-significant differences. Asterisks above each PCD denote the significance of the Kruskal–Wallis test for that metric at the corresponding PCD ($P < 0.05$, *$P < 0.01$, **$P < 0.001$; ns, not significant). Groups with low, medium, and high VSC are color-coded in red, yellow, and green, respectively.

1.3.2 Robustness of VSRE quantifying hierarchical coastal VSC with varying PCD

A common practical challenge is that researchers often cannot acquire LiDAR data with comparable point cloud densities across large study regions. To address this issue, we further pooled samples across all PCD levels to evaluate the robustness of different VSC metrics when applied to datasets with mixed PCD.

The statistical results showed that, under this mixed-PCD scenario, all VSC metrics significantly distinguished among the three structural complexity groups at a general level ($P < 0.001$). However, mean vegetation height, canopy cover, FHD, and canopy entropy consistently misclassified the medium-VSC group as having the lowest structural complexity (**Fig. 4a, b, c, e**, $P < 0.001$). Canopy surface roughness failed to differentiate between the low- and medium-VSC groups (**Fig. 4d**, $P < 0.001$). Although all metrics (except canopy cover) still significantly separated the low- and high-VSC groups, their discriminatory power was limited when differences in structural complexity were relatively small. This pattern indicates that commonly used VSC metrics exhibit low sensitivity in coastal wetlands dominated by herbaceous vegetation communities, particularly when PCD varies. In contrast, VSRE

https://doi.org/10.5194/essd-2026-68
Preprint. Discussion started: 23 March 2026
© Author(s) 2026. CC BY 4.0 License.

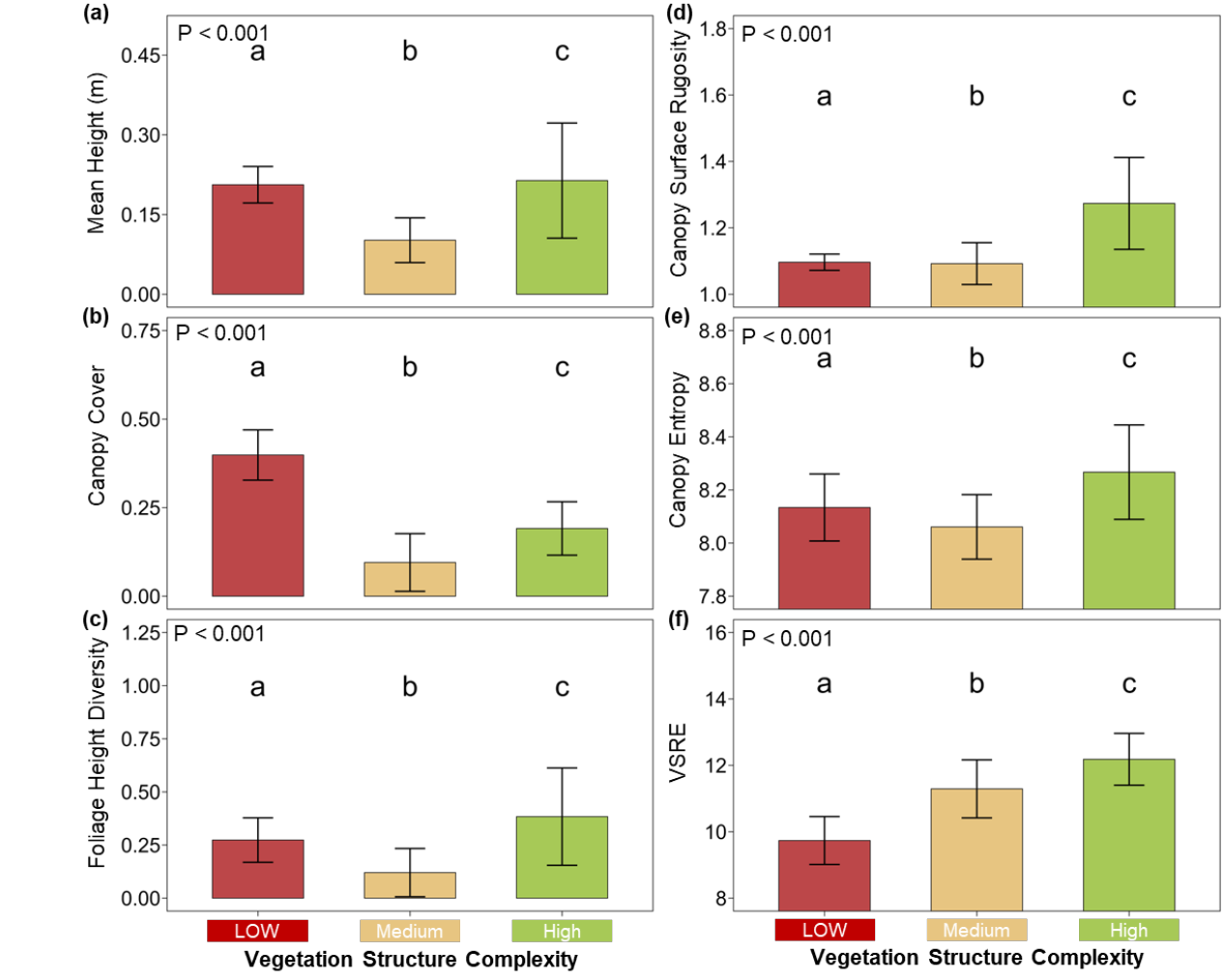

Fig. 4 | Comparison of the robustness of VSRE and other common VSC indicators with varying PCD. (a), mean vegetation height; **(b),** canopy cover; **(c)**, FHD (foliage height diversity); **(d)**, canopy rugosity; **(e)**, canopy surface entropy, and **(f)** VSRE. Bars indicate group means, and error bars denote the corresponding standard deviations. The Kruskal–Wallis test is applied to evaluate overall group differences, followed by Dunn's post hoc tests with Benjamin–Hochberg correction for pairwise comparisons. Different letters above boxes denote significant pairwise differences among groups. Groups with low, medium, and high VSC are color-coded in red, yellow, and green, respectively.

https://doi.org/10.5194/essd-2026-68
Preprint. Discussion started: 23 March 2026
© Author(s) 2026. CC BY 4.0 License.

Open Access Earth System Science Data Discussions

1.3.3 Effectiveness of VSRE quantifying VSC in a continuous gradient with varying PCD

Compared to the qualitative assessment of VSC by human observers, a more common phenomenon in natural vegetation communities is a continuously varying VSC. To address this, we used the Shannon diversity index, calculated based on biomass data, to simulate continuous changes in VSC within natural ecosystems. The original human-defined complexity classifications for the 18 plots were replaced with a quantitatively objective VSC, measured by the Shannon index, which quantifies the uniformity of vegetation biomass distributions within each plot.

Regression analyses indicated that commonly used vertical or horizontal VSC indicators, including vegetation height, canopy cover, and FHD, failed to capture the continuously varying structural complexity of coastal wetland vegetation (**Fig. 5a–c**, $P > 0.05$). Canopy entropy showed relatively better performance under high point cloud density conditions (**Fig. 5e**, $R^2 = 0.41^{**}$, PCD = 1500 pt m^{-2}), but its sensitivity markedly decreased at lower point cloud densities ($R^2 = 0.23$, PCD = 250 pt m^{-2}). In contrast, canopy surface roughness (**Fig. 5d**, $P < 0.01$) and VSRE (**Fig. 5f**, $P < 0.001$) exhibited clear linear relationships with vegetation structural complexity across all point cloud density levels. Moreover, VSRE achieved substantially higher goodness-of-fit than canopy roughness and consistently satisfied the assumption of normality, indicating a more stable, robust data structure.

https://doi.org/10.5194/essd-2026-68
Preprint. Discussion started: 23 March 2026
© Author(s) 2026. CC BY 4.0 License.

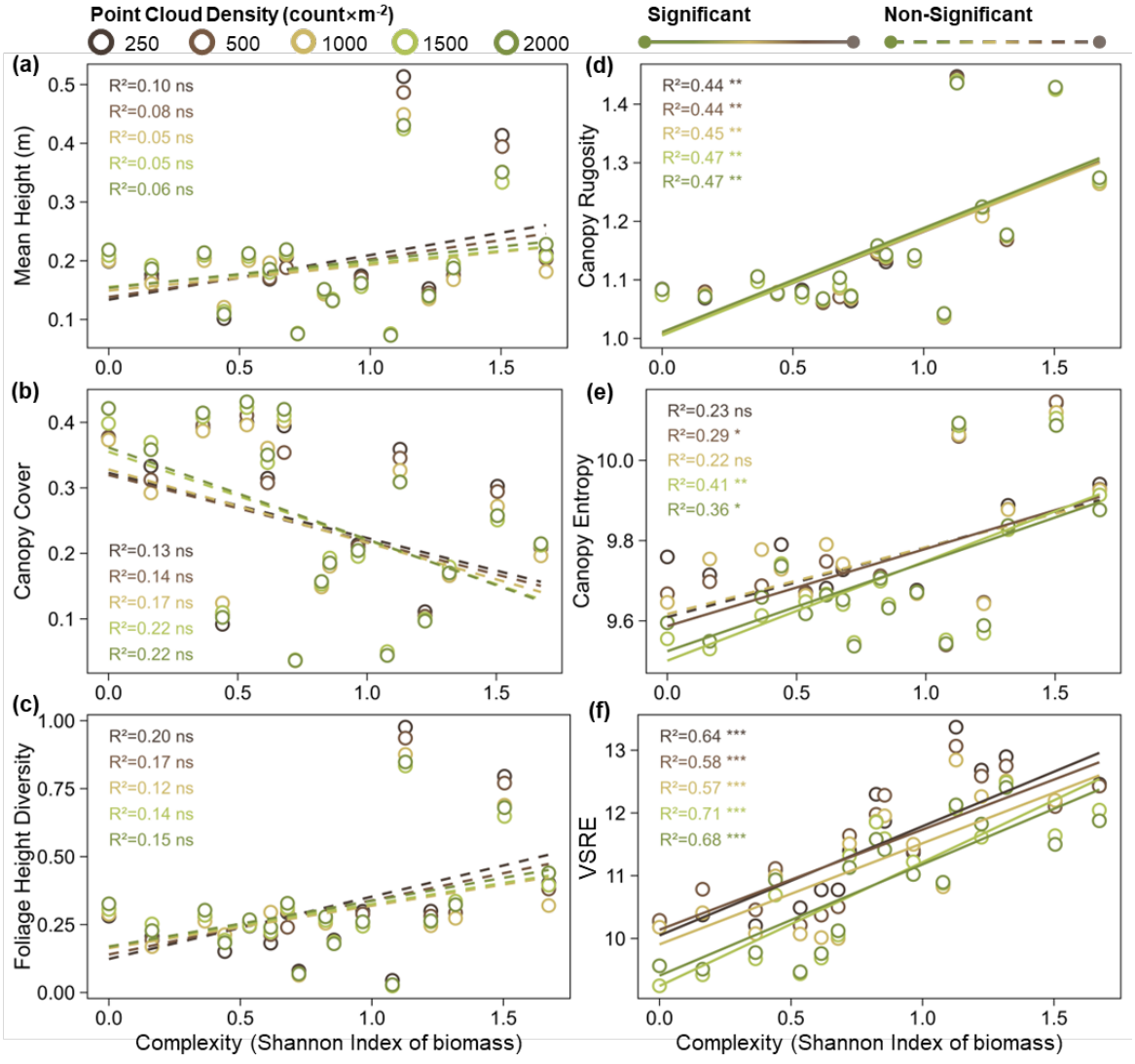

Fig. 5 | Linear trends in VSC indices with increasing quantitative complexity. (a), mean vegetation height; **(b),** canopy cover; **(c)**, FHD (foliage height diversity); **(d)**, canopy rugosity; **(e)**, canopy surface entropy, and **(f)** VSRE. Low-to-high point cloud densities are represented by a color gradient from dark brown to dark green. Statistical test results and methods are annotated on the left side of each subplot.

1.3.4 Structural diversity of natural vegetation in coastal China

We applied the VSRE algorithm to 1,337 LiDAR samples (each 25 × 25 m) collected from coastal regions of China. To accommodate the maximum potential height of mangroves in these areas (with 95% of individuals <10 m), we adjusted the maximum box height and Z-axis step size to 10 m and 0.5 m,

https://doi.org/10.5194/essd-2026-68
Preprint. Discussion started: 23 March 2026
© Author(s) 2026. CC BY 4.0 License.

Open Access Earth System Science Data Discussions

respectively. Additionally, we modified the scaling constant to $1e^{-43}$ to expand the VSRE values into a more interpretable 0–100 range (***Methods***).

The results revealed significant differences in VSRE among coastal vegetation communities ($P < 3.3\times10^{-111}$, **Fig. 6**). Mangrove communities exhibited the highest VSRE (median VSRE = 22.70), significantly exceeding the values observed in all other vegetation types. Graminoid-dominated communities, including *P. australis* marshes, mixed marshes, and *Spartina* spp. stands, showed intermediate VSRE values (median $VSRE_{P.\ australis}$ = 19.32, median $VSRE_{\text{mixed marshes}}$ = 13.19, median $VSRE_{Spartina\ \text{spp.}}$ = 11.49). Succulent-dominated (*Suaeda* spp.) and prostrate (*Scirpus* spp.) communities exhibited the lowest VSRE values (median $VSRE_{Scirpus\ \text{spp.}}$ = 7.90, median $VSRE_{Sueada\ \text{spp.}}$ = 5.77), with no significant difference between them. Moreover, vegetation types with higher median VSRE tended to exhibit greater variability in VSC values, suggesting greater structural heterogeneity. Nevertheless, the overall VSC of coastal vegetation remains much lower than that of terrestrial forest ecosystems ($VSRE_{forest}$ = 38.03, **Supplementary Table SS1**). Finally, robustness tests confirmed that adjusting the scaling constant did not alter the statistical relationships among indicators (**Supplementary Figure S4**).

https://doi.org/10.5194/essd-2026-68
Preprint. Discussion started: 23 March 2026
© Author(s) 2026. CC BY 4.0 License.

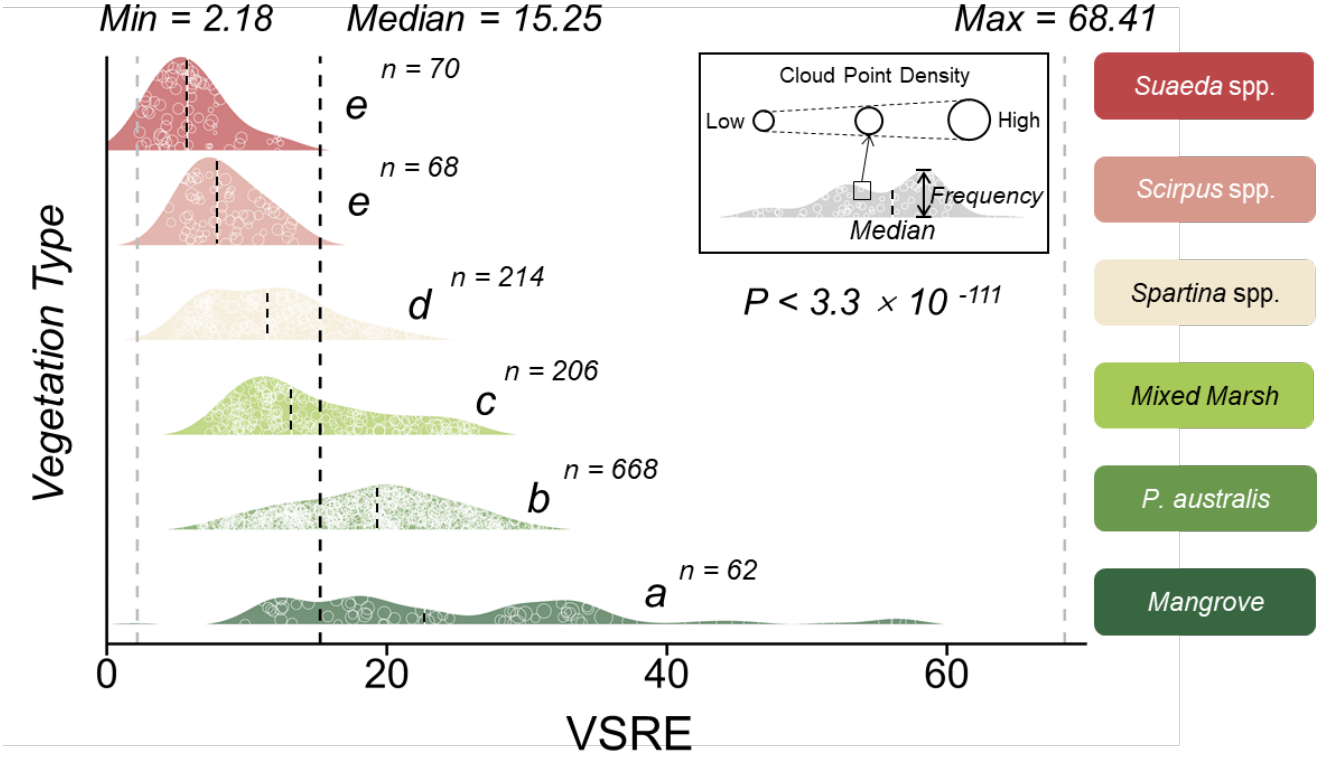

Fig. 6 | VSRE distributions across natural coastal vegetation communities. The frequency distributions of VSRE values for different plant communities are shown. Black dashed lines on a white background indicate the median VSRE for each vegetation community. White circles within the distribution curves represent the density of the sample point clouds. The overall median VSRE across all samples is also visualized with a black dashed line, while the grey curves indicate the maximum and minimum values observed. Kruskal–Wallis tests followed by Dunn's post hoc tests were used to assess significant differences in VSRE among vegetation communities.

1.3.5 Mapping wall-to-wall VSRE in coastal China

We incorporated the newly released AEF dataset (Brown et al., 2025), a dimensionless embedding of multidimensional spatial data (***Methods***). Using 1,337 laser quadrats collected in the field as training data, we employed a deep learning model (MLP) to generate a seamless spatial map of the VSRE for the Chinese coastal zone in 2022 at a 10 m resolution. Additionally, we conducted species-level

https://doi.org/10.5194/essd-2026-68
Preprint. Discussion started: 23 March 2026
© Author(s) 2026. CC BY 4.0 License.


vegetation classification for the coastal zone and mapped the average EVI during the growing season (**Fig. 7-8, 2**)(Qi et al., 2026).

The mapping results reveal significant shifts in vegetation community species composition from north to south along China's coast (**Fig. 7**). Low-latitude regions (20ºN~25ºN) are dominated by mangrove communities, while high-latitude regions (35ºN~40ºN) are primarily populated by *Suaeda spp.* and *P. australis*. Mid-latitude areas (25ºN~35ºN), particularly the Yangtze River Delta, exhibit richer species compositions and the largest expanses of coastal vegetation.

The VSRE mapping further describes the detailed spatial distribution of VSC. We observed a significant latitudinal gradient in VSC across China's coastal zones, with both the mean and the variance of vegetation structural complexity decreasing with increasing latitude. Estuarine regions, such as the Liaohe River Estuary, Yellow River Estuary, and Yangtze River Estuary, host coastal vegetation types with more complex structures, exhibiting higher VSRE variance compared to smoother coastlines. Zoom views of several coastal vegetation hotspots further emphasize the additional insights provided by VSRE mapping (**Fig. 8**). High spatial variability in VSRE was observed across multiple estuarine areas within the same vegetation type, revealing unexpected structural diversity influenced by tidal level and developmental age, which is hard to detect from a general observation method.

Overall, the quantification provided by VSRE enables researchers to move beyond species-level classifications and supports further quantitative analysis of VSC.

https://doi.org/10.5194/essd-2026-68
Preprint. Discussion started: 23 March 2026
© Author(s) 2026. CC BY 4.0 License.

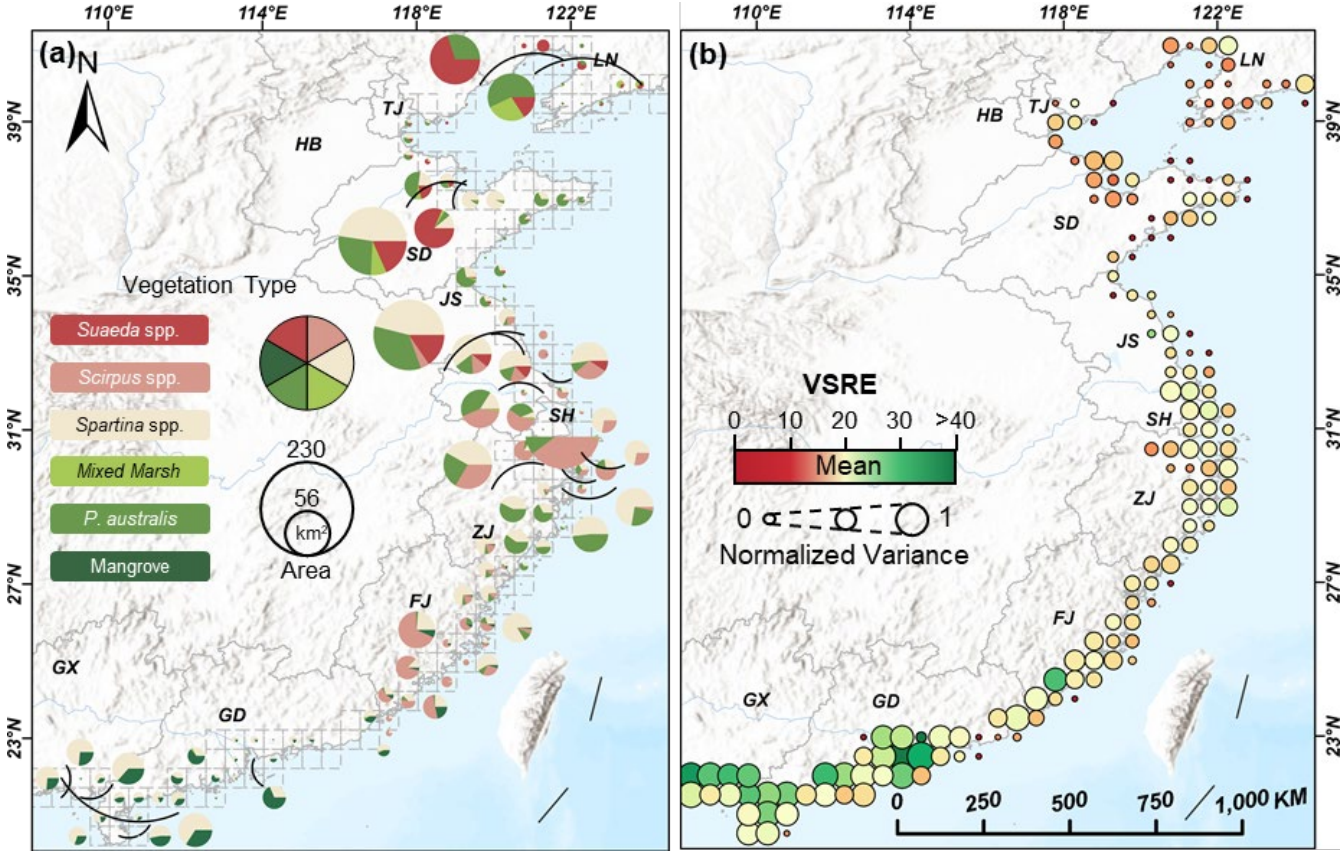

Fig. 7 | Spatial distribution of VSRE across coastal China. a, Vegetation composition across different coastal regions. The proportions of various vegetation types are illustrated using pie charts, with the sizes of the pie charts scaled to the total vegetation area within each 5° × 5° grid cell. **b**, Regional variation in VSRE. VSRE values are visualized using a color gradient from red (low complexity) to green (high complexity), while the circle sizes represent the normalized variance of VSRE within each 5° × 5° grid cell.

https://doi.org/10.5194/essd-2026-68
Preprint. Discussion started: 23 March 2026
© Author(s) 2026. CC BY 4.0 License.

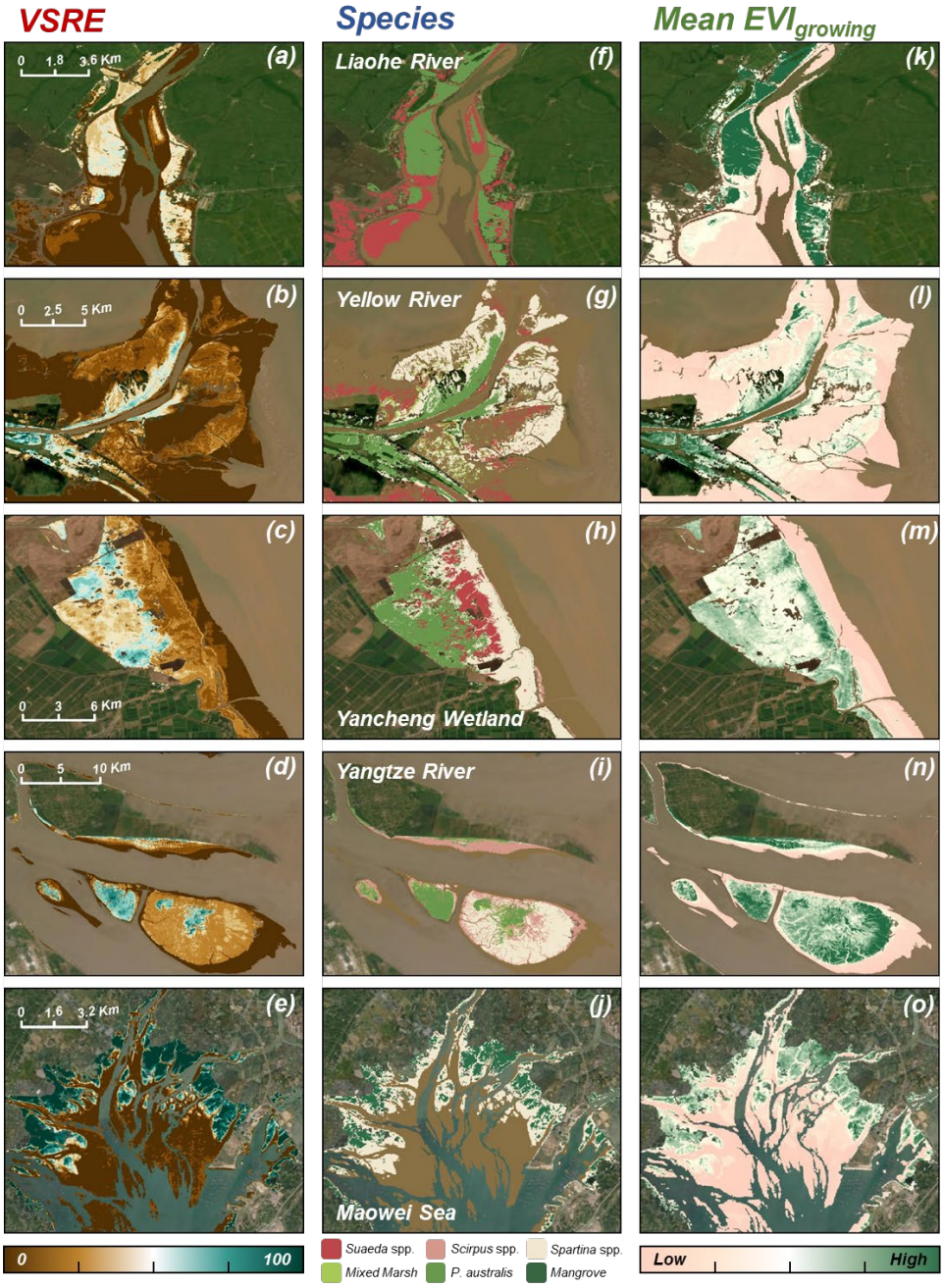

Fig. 8 | Comparison of VSRE with other widely used indicators for characterizing coastal wetlands. a-e, VSRE mapping, ranging from 0 to 100. **f-j,** main coastal vegetation mapping. **k-o,** mean EVI in the growing season of coastal vegetation (June ~ September, approximately ranging from 0 to 10).

https://doi.org/10.5194/essd-2026-68
Preprint. Discussion started: 23 March 2026
© Author(s) 2026. CC BY 4.0 License.

1.4 Discussion

1.4.1 Theoretical and practical advantages of VSRE in coastal wetlands

The concept of entropy originates from physics, where it describes the degree of disorder within a system. Since Shannon introduced it into information theory, information entropy has been widely applied in digital information processing(Cover and Thomas, 1991). More recently, following previous work using information entropy to point cloud data to quantify forest canopy complexity(Liu et al., 2022), many studies have been conducted in-depth analyses of the ecological functions and structural characteristics of forest canopies based on this concept(Liu et al., 2024; De Conto et al., 2024; Wang et al., 2023). However, a counterintuitive issue arises: the behaviour of information entropy does not align well with an intuitive understanding of VSC in ecological applications. The concept of information entropy in spatial point clouds is the accuracy with which points appear at specific spatial locations. Mathematically, the maximum value of information entropy occurs when the probability of the point cloud distribution is uniform across space, meaning a single point can appear randomly anywhere. Conversely, the minimum value occurs when all points are concentrated at a single location. This property implies that ecosystems typically regarded as having high VSC (e.g., mature forests) may exhibit lower calculated information entropy than ecosystems with relatively low VSC (e.g., secondary plantations). This inconsistency arises because informational disorder is not equivalent to structural disorder. In practice, before the point cloud reaches spatially saturated, the relationship between information entropy and VSC typically follows a unimodal curve, reaching a quadratic peak upon cloud point saturation (**Fig. 9**). This phenomenon explains why, in our results, the group exposed to high

https://doi.org/10.5194/essd-2026-68
Preprint. Discussion started: 23 March 2026
© Author(s) 2026. CC BY 4.0 License.

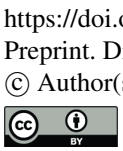

485 water levels, despite having significantly lower VSC, exhibited higher calculated CE and FHD values compared to the medium water level group with higher actual VSC (**Fig. 3b**).

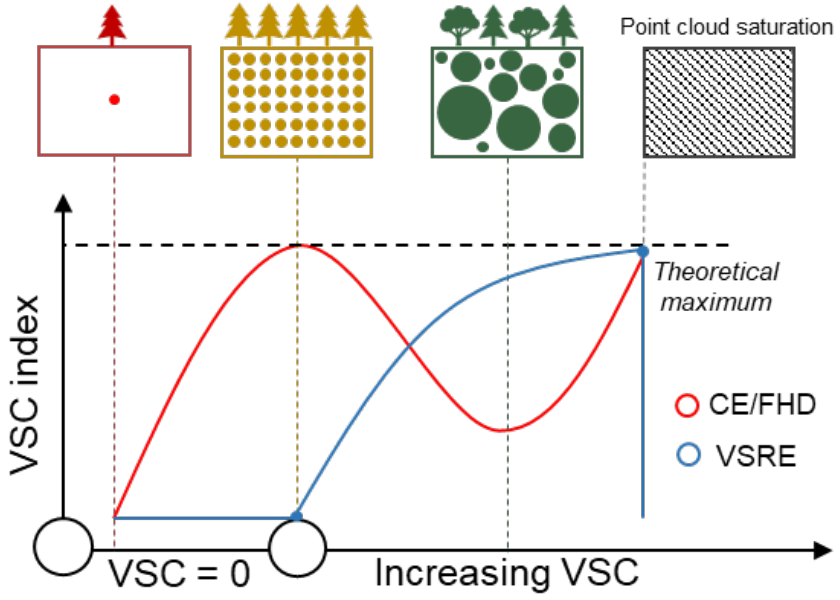

Fig. 9 | Theoretical trends of VSRE and CE/FHD as VSC increases.

490 RE differs from information entropy. RE measures the divergence between probability distributions, directly quantifying their differences(Baez and Pollard, 2016). Our approach uses regionalized point cloud data to generate multiple discrete spatial distributions, allowing us to assess the overall structural similarity. This method aligns closely with our intuitive understanding of VSC; greater structural reproducibility indicates lower VSC. Moreover, VSRE is computationally efficient. 495 Rather than relying on kernel density estimation, VSRE performs discrete frequency statistics within voxelized boxes, greatly enhancing processing speed. In testing, we found that for a single 25 × 25 m LiDAR sample, VSRE operated at approximately 10 times the efficiency of the CE algorithm, with computational efficiency increasing nearly exponentially as point cloud density rises (**Supplementary**

https://doi.org/10.5194/essd-2026-68
Preprint. Discussion started: 23 March 2026
© Author(s) 2026. CC BY 4.0 License.


Figure S5). This high computational efficiency enables direct comparison of the original 3D point cloud's structural distributions without preprocessing steps such as resampling or projection, which can otherwise degrade information fidelity. As a result, VSRE significantly improves model sensitivity to subtle structural differences. Finally, VSRE provides a rich set of adjustable parameters and robust responses to point cloud characteristics, particularly regarding the step size and maximum height in the Z direction. Researchers can fine-tune these parameters to detect VSC differences across ecosystems with varying structural traits, provided that the sample size is sufficiently large or that point cloud densities are comparable in magnitude.

1.4.2 VSC of coastal wetlands in China

By deploying the VSRE algorithm across 1,337 LiDAR samples collected along coastal China and integrating species-level vegetation classification mapping, we achieved a comprehensive understanding of VSC at both the species and regional scales (**Fig. 4-6, Supplementary Table S2**).

Our mapping revealed significant differences in VSC among coastal vegetation types, not only between different species but also within the same species across different regions. Differences in VSC among species may be attributed to variations in productivity, stress resistance, and growth cycles(Qi et al., 2024; Kirwan and Megonigal, 2013; Duarte et al., 2013; Mathis et al., 2024). Mangrove communities, characterized by high productivity and extended growth cycles(Rovai et al., 2018), exhibited higher VSC, while *Scirpus* spp. and *Suaeda* spp., which allocate more resources toward stress resistance, demonstrated relatively lower VSC(Lafond-Hudson and Sulman, 2023; Sun et al., 2022). Intraspecific differences in VSC appear to be influenced by local growth conditions and human disturbance. For example, *P. australis*, a species widely distributed along China's coast, exhibited the

https://doi.org/10.5194/essd-2026-68
Preprint. Discussion started: 23 March 2026
© Author(s) 2026. CC BY 4.0 License.


highest mean VSC in Shanghai ($VSRE_{mean}$ = 21.84), surpassing even the mangroves in Guangxi ($VSRE_{mean}$ = 20.92). It can be attributed to the dominance of *P. australis* in the long-protected Dongtan National Wetland in Shanghai, where favorable conditions support more structurally complex growth(Qi et al., 2024).

Additionally, the range of VSC within species is likely associated with the plants' intrinsic growth characteristics. Mangroves, with growth cycles of 5 to 10 years, can exhibit substantial structural variation among individuals of different ages, as in terrestrial forests, resulting in a wide range of VSRE values. In contrast, most salt marsh plants exhibit relatively simple, repetitive growth forms, resulting in unimodal frequency distributions of VSRE (Lafond-Hudson and Sulman, 2023). It is noteworthy that previous studies have shown that intertidal ecosystems often lack latitudinal diversity gradients (Thyrring and Harley, 2024), a conclusion supported by our coastal vegetation species mapping (**Fig. 5**). However, VSC, as characterized by VSRE, exhibits a transparent latitudinal gradient in both mean and variance (**Fig. 6**). This discrepancy suggests that structural complexity may be a more suitable and universally applicable functional characteristic for both terrestrial and marine ecosystems.

1.4.3 Limitations and Uncertainties

Although VSRE offers significant advantages in principle and computational efficiency, it still presents several limitations that should not be overlooked. First, a necessary prerequisite must be emphasized: the information purity of point cloud data. Specifically, the spatial distribution of the point cloud should accurately reflect the vegetation's actual structure, without significant distortion from sampling methods or external factors. A major challenge in applying VSRE to airborne or satellite-borne laser data is the potential information distortion caused by dense canopy cover, which may impact modelling

https://doi.org/10.5194/essd-2026-68
Preprint. Discussion started: 23 March 2026
© Author(s) 2026. CC BY 4.0 License.


accuracy(Wulder et al., 2012). In this study, the application of VSRE in coastal ecosystems with inherently open canopies minimizes concerns about canopy-induced data distortion. However, we argue that correcting canopy oversampling in CE algorithms using resampling methods may not be appropriate. Since forest structures are typically dense at the canopy and sparse near the ground, resampling can remove key information and introduce noise. Further empirical validation is required to determine whether such corrections can effectively balance noise reduction and information retention.

In addition, algorithms based on RE face two theoretical limitations, although these conditions are rarely encountered in natural ecosystems. When VSC is exceptionally high, and the spatial point cloud becomes saturated, RE values may decrease sharply toward zero. Additionally, when structures involve simple rearrangements of identical elements, such as clusters of uniform vegetation point clouds distributed across different spatial locations, RE may be unable to differentiate them due to the isentropic nature of such configurations. Finally, we acknowledge that the calculation of VSRE remains sensitive to point cloud density. Although this sensitivity diminishes substantially with a large sample size, we recommend using laser datasets with comparable point cloud densities (preferably >250 points/m^2) to ensure reliable analysis results.

1.4.4 Implications and Conclusions

Drawing on the world's largest water-level control experiment and the most comprehensive LiDAR dataset of China's coastal zone, this study developed the VSRE index based on the concept of RE to effectively quantify the complexity of coastal VSC. Compared to the currently used VSC index, VSRE offers clear advantages in theoretical foundation, computational efficiency, and range of application. It enables the detailed characterization of VSC within coastal plant communities. Our findings advance the understanding of growth characteristics in coastal vegetation and provide an essential scientific basis for developing sustainable coastal management

https://doi.org/10.5194/essd-2026-68
Preprint. Discussion started: 23 March 2026
© Author(s) 2026. CC BY 4.0 License.


policies. Furthermore, given the critical ecosystem services they provide, this study underscores the urgent need to address the underrepresentation of coastal wetlands in current land-surface models.

https://doi.org/10.5194/essd-2026-68
Preprint. Discussion started: 23 March 2026
© Author(s) 2026. CC BY 4.0 License.

Code availability

The VSRE code used in this study is openly available from GitHub at https://github.com/EmpTyset-phi/VSRE.

Data availability

The datasets described in this manuscript are deposited in figshare *https://doi.org/10.6084/m9.figshare.30588722* under a CC BY 4.0 licence (Qi et al., 2026). The repository contains the 2022 wall-to-wall VSRE map for coastal China at 10 m spatial resolutione. All deposited files are provided in open, non-proprietary formats. Third-party input datasets used in this study, including the Alpha Earth Foundation embeddings and satellite imagery products, are available from their original providers and are therefore not redistributed in this repository.

Supplementary Materials

Supplementary Materials are available for this paper, including Figures S1 to S6, and Tables S1 to S5. The link to the supplement will be included by Copernicus.

Author contributions

J.M. and X.C. conceived the idea. G.P.Q., J.W.W., Z.Z.X., and L.C.Y. performed the research. G.P.Q. and J.W.W. analyzed the data and made the visualizations. G.P.Q. and J.W.W. wrote the first draft with help from J.M. and X.C..

Competing interests

The authors declare no competing interests.

Acknowledgements

We sincerely thank Keryn Gedan from George Washington University for her contribution to improving the first draft. We also acknowledge the support and assistance provided by the CFFF Intelligent Computing Platform of Fudan University.

Financial support

This research was supported by the Natural Science Foundation of China (32271659), and the Scientific Research Program of Shanghai Science and Technology Commission (23DZ1204504), and State Key Laboratory of Wetland Conservation and Restoration-Wetland Young Scientist Program (SDGZ-QN2025-03).

https://doi.org/10.5194/essd-2026-68
Preprint. Discussion started: 23 March 2026
© Author(s) 2026. CC BY 4.0 License.

References

Atkins, J. W., Bohrer, G., Fahey, R. T., Hardiman, B. S., Morin, T. H., Stovall, A. E., Zimmerman, N., and Gough, C. M.: Quantifying vegetation and canopy structural complexity from terrestrial Li DAR data using the forestr r package, Methods Ecol. Evol., 9, 2057-2066, 2018.

Baez, J. C. and Pollard, B. S.: Relative entropy in biological systems, Entropy, 18, 46, 2016.

Bergen, K., Goetz, S., Dubayah, R., Henebry, G., Hunsaker, C., Imhoff, M., Nelson, R., Parker, G., and Radeloff, V.: Remote sensing of vegetation 3 - D structure for biodiversity and habitat: Review and implications for lidar and radar spaceborne missions, J. Geophys. Res.: Biogeosci., 114, 2009.

Breiman, L.: Random forests, Mach. Learn., 45, 5-32, 10.1007/978-3-030-56485-8_3, 2001.

Chambers, J. Q., Asner, G. P., Morton, D. C., Anderson, L. O., Saatchi, S. S., Espírito-Santo, F. D., Palace, M., and Souza, C.: Regional ecosystem structure and function: ecological insights from remote sensing of tropical forests, Trends Ecol. Evol., 22, 414-423, 2007.

Chen, J., Jönsson, P., Tamura, M., Gu, Z., Matsushita, B., and Eklundh, L.: A simple method for reconstructing a high-quality NDVI time-series data set based on the Savitzky–Golay filter, Remote Sens. Environ., 91, 332-344, 10.1016/s0034-4257(04)00080-x, 2004.

Costanza, R., d'Arge, R., De Groot, R., Farber, S., Grasso, M., Hannon, B., Limburg, K., Naeem, S., O'neill, R. V., and Paruelo, J.: The value of the world's ecosystem services and natural capital, Nature, 387, 253-260, 1997.

Cousins, S. H.: Species diversity measurement: choosing the right index, Trends Ecol. Evol., 6, 190-192, 1991.

Cover, T. M. and Thomas, J. A.: Entropy, relative entropy and mutual information, Elements of information theory, 2, 12-13, 1991.

Dassot, M., Constant, T., and Fournier, M.: The use of terrestrial LiDAR technology in forest science: application fields, benefits and challenges, Ann. For. Sci., 68, 959-974, 2011.

de Conto, T., Armston, J., and Dubayah, R.: Characterizing the structural complexity of the Earth's forests with spaceborne lidar, Nat. Commun., 15, 8116, 2024.

Drusch, M., Del Bello, U., Carlier, S., Colin, O., Fernandez, V., Gascon, F., Hoersch, B., Isola, C., Laberinti, P., and Martimort, P.: Sentinel-2: ESA's optical high-resolution mission for GMES operational services, Remote Sens. Environ., 120, 25-36, 10.1016/j.rse.2011.11.026, 2012.

Duarte, C. M., Losada, I. J., Hendriks, I. E., Mazarrasa, I., and Marbà, N.: The role of coastal plant communities for climate change mitigation and adaptation, Nat. Clim. Change, 3, 961-968, 10.1038/nclimate1970, 2013.

Ehbrecht, M., Seidel, D., Annighöfer, P., Kreft, H., Köhler, M., Zemp, D. C., Puettmann, K., Nilus, R., Babweteera, F., and Willim, K.: Global patterns and climatic controls of forest structural complexity, Nat. Commun., 12, 519, 2021.

Fischer, F. J., Maréchaux, I., and Chave, J.: Improving plant allometry by fusing forest models and remote sensing, New Phytol., 223, 1159-1165, 2019.

https://doi.org/10.5194/essd-2026-68
Preprint. Discussion started: 23 March 2026
© Author(s) 2026. CC BY 4.0 License.

Frantz, D., Haß, E., Uhl, A., Stoffels, J., and Hill, J.: Improvement of the Fmask algorithm for Sentinel-2 images: Separating clouds from bright surfaces based on parallax effects, Remote Sens. Environ., 215, 471-481, 10.1016/j.rse.2018.04.046, 2018.

Gorelick, N., Hancher, M., Dixon, M., Ilyushchenko, S., Thau, D., and Moore, R.: Google Earth Engine: Planetary-scale geospatial analysis for everyone, Remote Sens. Environ., 202, 18-27, 10.1016/j.rse.2017.06.031, 2017.

He, Q., Li, Z. a., Daleo, P., Lefcheck, J. S., Thomsen, M. S., Adams, J. B., and Bouma, T. J.: Coastal wetland resilience through local, regional and global conservation, Nat. Rev. Biodivers., 1, 50-67, 10.1038/s44358-024-00004-x, 2025.

Holling, C. S.: Simplifying the complex: the paradigms of ecological function and structure, Eur. J. Oper. Res., 30, 139-146, 1987.

Irons, J. R., Dwyer, J. L., and Barsi, J. A.: The next Landsat satellite: The Landsat data continuity mission, Remote Sens. Environ., 122, 11-21, 10.1016/j.rse.2011.08.026, 2012.

Jucker, T., Fischer, F. J., Chave, J., Coomes, D. A., Caspersen, J., Ali, A., Loubota Panzou, G. J., Feldpausch, T. R., Falster, D., and Usoltsev, V. A.: Tallo: A global tree allometry and crown architecture database, Global Change Biol., 28, 5254-5268, 2022.

Kirwan, M. L. and Megonigal, J. P.: Tidal wetland stability in the face of human impacts and sea-level rise, Nature, 504, 53-60, 10.1038/nature12856, 2013.

LaFond‐Hudson, S. and Sulman, B.: Modeling strategies and data needs for representing coastal wetland vegetation in land surface models, New Phytol., 238, 938-951, 10.1111/nph.18760, 2023.

Liu, X., Ma, Q., Wu, X., Hu, T., Liu, Z., Liu, L., Guo, Q., and Su, Y.: A novel entropy-based method to quantify forest canopy structural complexity from multiplatform lidar point clouds, Remote Sens. Environ., 282, 113280, 2022.

Liu, X., Feng, Y., Hu, T., Luo, Y., Zhao, X., Wu, J., Maeda, E. E., Ju, W., Liu, L., and Guo, Q.: Enhancing ecosystem productivity and stability with increasing canopy structural complexity in global forests, Sci. Adv., 10, eadl1947, 2024.

Lohani, B. and Ghosh, S.: Airborne LiDAR technology: A review of data collection and processing systems, Proc. Natl. Acad. Sci., India, Sect. A Phys. Sci., 87, 567-579, 2017.

Loreau, M., Naeem, S., Inchausti, P., Bengtsson, J., Grime, J. P., Hector, A., Hooper, D. U., Huston, M. A., Raffaelli, D., Schmid, B., Tilman, D., and Wardle, D. A.: Biodiversity and ecosystem functioning: current knowledge and future challenges, Science, 294, 804-808, 10.1126/science.1064088, 2001.

MacArthur, R. H. and MacArthur, J. W.: On bird species diversity, Ecology, 42, 594-598, 1961.

Mathis, M., Lacroix, F., Hagemann, S., Nielsen, D. M., Ilyina, T., and Schrum, C.: Enhanced CO2 uptake of the coastal ocean is dominated by biological carbon fixation, Nat. Clim. Change, 14, 373-379, 2024.

Mcleod, E., Chmura, G. L., Bouillon, S., Salm, R., Björk, M., Duarte, C. M., Lovelock, C. E., Schlesinger, W. H., and Silliman, B. R.: A blueprint for blue carbon: toward an improved understanding of the role of vegetated coastal habitats in sequestering CO2, Front. Ecol. Environ., 9, 552-560, 10.1890/110004, 2011.

Moffett, K. B., Nardin, W., Silvestri, S., Wang, C., and Temmerman, S.: Multiple stable states and catastrophic shifts in

https://doi.org/10.5194/essd-2026-68
Preprint. Discussion started: 23 March 2026
© Author(s) 2026. CC BY 4.0 License.

coastal wetlands: Progress, challenges, and opportunities in validating theory using remote sensing and other methods, Remote Sens., 7, 10184-10226, 2015.

Parker, G. G. and Russ, M. E.: The canopy surface and stand development: assessing forest canopy structure and complexity with near-surface altimetry, For. Ecol. Manage., 189, 307-315, 2004.

Pinkus, A.: Approximation theory of the MLP model in neural networks, Acta Numer., 8, 143-195, 1999.

Qi, G., Wei, J., Li, H., Xie, T., Li, L., Wang, F., He, Q., Mudd, S. M., and Ma, J.: Insight into rapid vegetation dynamics in China's saltmarshes reveals overlooked coastal soil carbon storage, One Earth, 9, 2026.

Qi, G., Li, L., Li, H., Liu, Y., Xie, T., Guo, H., Ma, Z., Wu, J., Li, B., and Ma, J.: Ecological Effects of the Huge Invasive Species Removal Project in Coastal China, Environ. Sci. Technol., 2024.

Qi, Guanpu; Wei, Jiawei; Xin, Zaizhou; Yao, Longcheng; Chen, Xiong; Ma, Jun (2026). VSRE mapping data for "Revealing coastal vegetation structural diversity through LiDAR-derived relative entropy". figshare. Dataset. https://doi.org/10.6084/m9.figshare.30588722

Robinson, C. J., Bohannan, B. J., and Young, V. B.: From structure to function: the ecology of host-associated microbial communities, Microbiol. Mol. Biol. Rev., 74, 453-476, 2010.

Rovai, A. S., Twilley, R. R., Castañeda-Moya, E., Riul, P., Cifuentes-Jara, M., Manrow-Villalobos, M., Horta, P. A., Simonassi, J. C., Fonseca, A. L., and Pagliosa, P. R.: Global controls on carbon storage in mangrove soils, Nat. Clim. Change, 8, 534-538, 10.1038/s41558-018-0162-5, 2018.

Simard, M., Fatoyinbo, L., Smetanka, C., Rivera-Monroy, V. H., Castañeda-Moya, E., Thomas, N., and Van der Stocken, T.: Mangrove canopy height globally related to precipitation, temperature and cyclone frequency, Nat. Geosci., 12, 40-45, 2019.

Sun, B., Jiang, M., Han, G., Zhang, L., Zhou, J., Bian, C., Du, Y., Yan, L., and Xia, J.: Experimental warming reduces ecosystem resistance and resilience to severe flooding in a wetland, Sci. Adv., 8, eabl9526, 10.1126/sciadv.abl9526, 2022.

Tang, H., Armston, J., Hancock, S., Marselis, S., Goetz, S., and Dubayah, R.: Characterizing global forest canopy cover distribution using spaceborne lidar, Remote Sens. Environ., 231, 111262, 2019.

Temmerman, S., Meire, P., Bouma, T. J., Herman, P. M., Ysebaert, T., and De Vriend, H. J.: Ecosystem-based coastal defence in the face of global change, Nature, 504, 79-83, 10.1038/nature12859, 2013.

Theiler, J.: Estimating fractal dimension, Journal of the optical society of America A, 7, 1055-1073, 1990.

Thyrring, J. and Harley, C. D.: Marine latitudinal diversity gradients are generally absent in intertidal ecosystems, Ecology, 105, e4205, 2024.

Wang, X., Rahman, M. A., Mokroš, M., Rötzer, T., Pattnaik, N., Pang, Y., Zhang, Y., Da, L., and Song, K.: The influence of vertical canopy structure on the cooling and humidifying urban microclimate during hot summer days, Landscape Urban Plann., 238, 104841, 2023.

Wulder, M. A., White, J. C., Nelson, R. F., Næsset, E., Ørka, H. O., Coops, N. C., Hilker, T., Bater, C. W., and Gobakken, T.: Lidar sampling for large-area forest characterization: A review, Remote Sens. Environ., 121, 196-209, 2012.

Yando, E. S., Jones, S. F., James, W. R., Colombano, D. D., Montemayor, D. I., Nolte, S., Raw, J. L., Ziegler, S. L., Chen, L.,

https://doi.org/10.5194/essd-2026-68
Preprint. Discussion started: 23 March 2026
© Author(s) 2026. CC BY 4.0 License.

and Daffonchio, D.: An integrative salt marsh conceptual framework for global comparisons, Limnol. Oceanogr. Lett., 8, 830-849, 10.1002/lol2.10346, 2023.